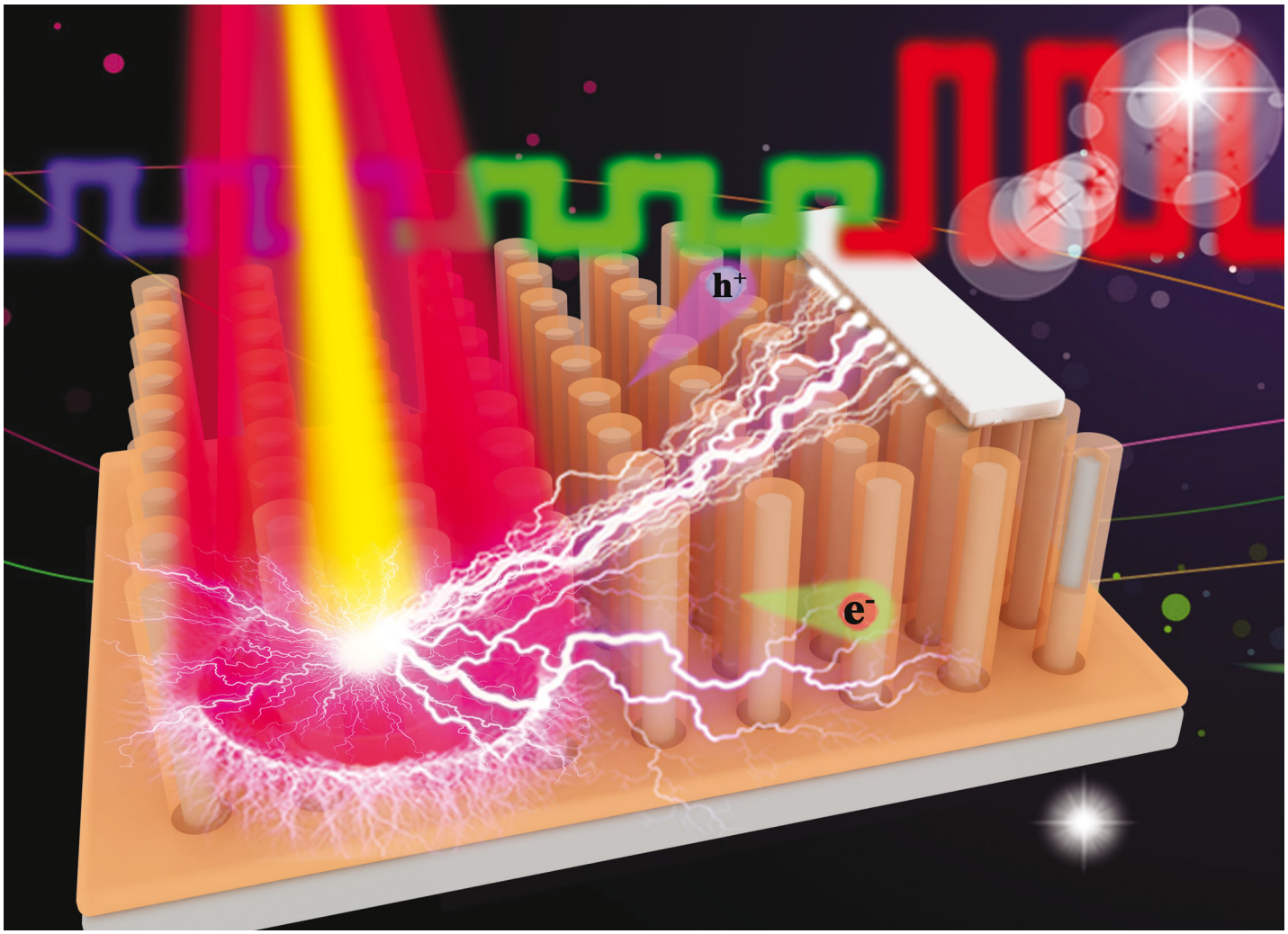

Showcasing research from Professor Lin-Bao Luo and colleagues at Hefei University of Technology, China.

Core–shell silicon nanowire array–Cu nanofilm Schottky junction for a sensitive self-powered near-infrared photodetector

A highly sensitive photodetector was fabricated by depositing silicon nanowire array with Cu nanoparticle films. The as-fabricated device displayed obvious sensitivity to near infrared light with good reproducibility and stability.

As featured in:

See Lin-Bao Luo *et al.*, *J. Mater. Chem. C*, 2016, **4**, 10804.

ROYAL SOCIETY OF CHEMISTRY

www.rsc.org/MaterialsC

Registered charity number: 207890

Journal of Materials Chemistry C

PAPER

View Article Online
View Journal | View Issue

Cite this: J. Mater. Chem. C, 2016, 4, 10804

Core–shell silicon nanowire array–Cu nanofilm Schottky junction for a sensitive self-powered near-infrared photodetector†

Chun-Yan Wu, Zhi-Qiang Pan, You-Yi Wang, Cai-Wang Ge, Yong-Qiang Yu, Ji-Yu Xu, Li Wang and Lin-Bao Luo*

Received 5th September 2016,
Accepted 26th October 2016

DOI: 10.1039/c6tc03856e

www.rsc.org/MaterialsC

A highly sensitive near infrared light (NIR) photodetector was fabricated by coating a thin layer of Cu film onto a vertical n-type SiNW array through a solution based reduction reaction. The as-fabricated core–shell SiNW array/Cu Schottky junction exhibits an obvious rectifying behavior in the dark with a turn-on voltage of ~0.5 V and a rectification ratio of about 10^2 at ±1.5 V. In addition, it shows a pronounced photovoltaic performance when illuminated by NIR light with a wavelength of 980 nm. Such photovoltaic characteristics can allow the device to detect NIR illumination without exterior power supply. Further device analysis reveals that the self-powered NIR photodetector is capable of monitoring ultrafast optical signals with a frequency as high as 30 kHz. What is more, the present device also has obvious advantages of high responsivity, detectivity, on/off ratio, and response speed. Further theoretical simulation reveals that the good device performance is associated with excellent optical and electrical properties of core–shell heterojunction geometry.

1. Introduction

Infrared (IR) light, as electromagnetic radiation with a longer wavelength than visible light, has been widely used for various military applications including target acquisition, surveillance and night vision,[1–3] as well as non-military purposes such as thermal efficiency analysis, remote temperature sensing, and environmental monitoring.[4,5] A number of narrow bandgap semiconductors, *e.g.* PbS, InSb, CdZnTe, GaAs and Si, have been selected for the fabrication of IR photodetectors.[6] Among the various IR devices, the CMOS-compatible Si photodetectors have attracted considerable research attention.[7–9] To date, a variety of Si-based IR photodetectors with different device geometries, including Schottky diodes,[10] p–n diodes,[11] p–i–n diodes,[12] and back-to-back metal–semiconductor–metal (MSM) Schottky junction photodetectors,[13] have been realized. Comparatively, Schottky junction based IR photodetectors have been of particular interest because of their obvious advantages of simple device architecture, fast response speed and small parasitic capacitance.

In comparison to thin film and bulk based photodetectors, devices made of semiconductor nanostructures often exhibit obvious advantages of high sensitivity, low energy consumption and high response speed in that their low reflectance and high surface-to-volume ratio lead to increased photon collection efficiency and the low dimensions of the effective conductive channel shorten the transit times of the carriers.[14] By this token, one-dimensional Si (1D) nanostructures, in particular Si nanowires with a strong light-trapping effect, have received enormous research interest in the field of high-performance IR photodetectors. For instance, Cao *et al.* reported a broad spectrum photodetector by forming an RGO–SiNW array heterojunction *via* simple drop-casting of the suspension of GO nanosheets on top of the SiNW array. The photodetector achieves high sensitivity detection of the infrared radiation from the human body with good device reproducibility.[15] Our group recently also developed a high performance near infrared light photodetector by decorating graphene–SiNWs with plasmonic gold nanoparticles.[16] The on/off ratio is as high as 10^6, which is much higher than other Si nanostructure based devices. What is more, the responsivity and detectivity of the device were estimated to be 1.5 A W^{-1} and 2.52 × 10^{14} cm $Hz^{1/2}$ W^{-1}, respectively. By coating a freestanding SiNW array with a layer of carbon quantum dots, the as-assembled devices are capable of high-frequency optical signals with a high relative balance. Furthermore, the response speed is around 20 microseconds, which is comparable to that of commercial Si-based photodetectors.[17] Enlightened by the above study, we herein report a core–shell SiNW array/Cu nanofilm Schottky junction NIR photodetector. The device was fabricated by coating the surface

School of Electronic Science and Applied Physics, Hefei University of Technology, Hefei, Anhui 230009, China. E-mail: luolb@hfut.edu.cn

† Electronic supplementary information (ESI) available. See DOI: 10.1039/c6tc03856e

of a freestanding SiNW array with a layer of Cu, which is known to be an important metallization material for microelectronic devices due to its low resistivity and high electromigration resistance. Thanks to the strong light-trapping effect of the SiNW array and the encapsulation of the Cu thin film on the surface of SiNWs, the as-fabricated NIR photodetector exhibits typical rectifying behavior with a rectifying ratio of 10^2. Further device analysis reveals that the near IR (NIR) photodetector is capable of detecting 980 nm illumination with excellent reproducibility and stability, and fast response speed. The responsivity and detectivity were estimated to be 0.335 A W^{-1} and 2.9×10^{12} cm $Hz^{1/2}$ W^{-1}, respectively.

2. Results and discussion

The proof-of-concept core–shell SiNW array/Cu nanofilm Schottky junction NIR photodetector (Fig. 1a) was fabricated by coating a thin layer of Cu film onto the surface of a freestanding n-type SiNW array with an average length of ~4 μm and an average diameter of ~150 nm (mostly 100–300 nm, as shown in Fig. 1b), which was synthesized through a metal nanoparticle assisted HF etching method. The step-wise flowchart for the fabrication of the NIR device is shown in Fig. S1, ESI.† Fig. 1c shows a typical field emission scanning electron microscopy (FESEM) image of the SiNW array that was functionalized by a layer of Cu nano-thin film. According to the XRD pattern, the EDS spectrum (Fig. S2 and S3, ESI†), and high-resolution transmission electron microscopy (HRTEM) image shown in Fig. 1d, the shell layer can be readily ascribed to face-centered cubic Cu (JCPDS card no. 04-836). As a matter of fact, the core–shell geometry can be further confirmed by the TEM image (Fig. 1e), and the corresponding elemental mapping images (Fig. 1f and g), in which the nanowire is constituted by a Si core and a Cu shell with a thickness of about 15 nm.

The typical current (I)–voltage (V) curve of the core–shell SiNW array/Cu Schottky junction in the dark is shown in Fig. 2a, revealing an obvious rectifying behavior with a turn-on voltage of ~0.5 V and a rectification ratio of about 10^2 at ±1.5 V. The barrier height of such SiNW array/Cu is estimated to be 0.66 eV

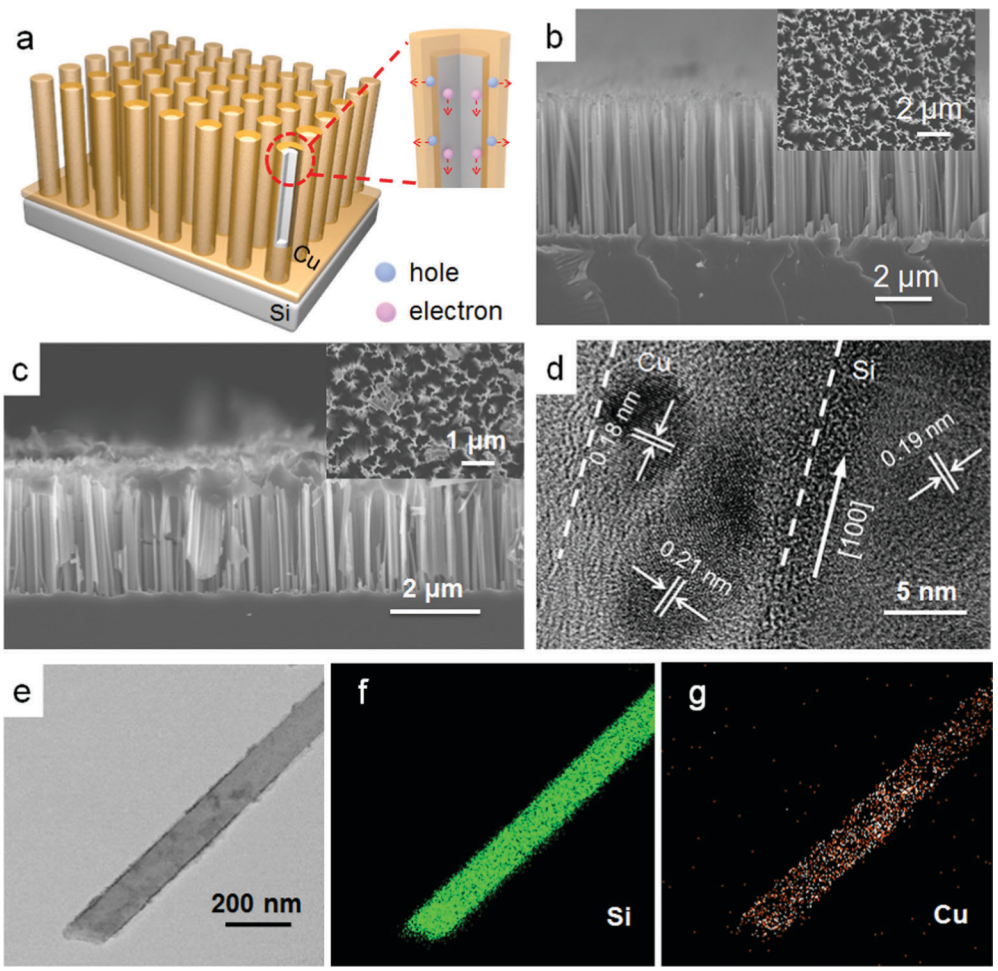

Fig. 1 (a) Schematic illustration of the core–shell SiNW array/Cu Schottky junction. Cross-sectional FESEM images of the SiNW array (b) before and (c) after the deposition of Cu film, the insets show the corresponding bird's eye view of FESEM images. (d) HRTEM image of the core–shell SiNW array/Cu Schottky junction. (e) TEM image and the corresponding elemental mapping of (f) Si and (g) Cu of a typical core–shell nanostructure which was scraped from the SiNW array after the deposition of Cu nano thin film.

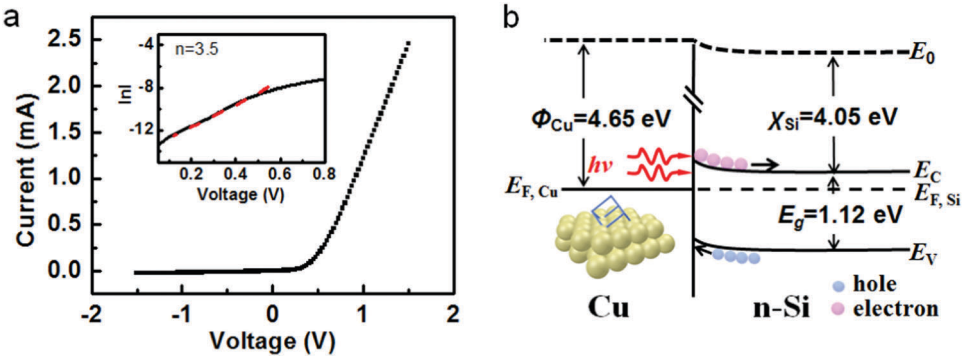

Fig. 2 (a) The typical current (I)–voltage (V) curve of the core–shell SiNW array/Cu nanofilm Schottky junction in the dark, the inset presents the plot of $\ln I - V$, showing the ideality factor of the device. (b) Energy-band diagram of the Si/Cu Schottky junction under illumination at zero bias. Φ_{Cu} denotes the work function of Cu. χ_{Si} denotes the electron affinity of Si. $E_{F,Cu}$ and $E_{F,Si}$ denote the Fermi energy levels of Cu and Si, respectively. E_C, E_V and E_g represent the conduction band, valence band, and band-gap of Si, respectively. E_0 is the vacuum energy level.

(see the ESI†), comparable to that of the SiNW array/graphene interface.[16] Moreover, the diode ideality factor (n) is estimated to be 3.5 according to the $\ln I$–V curve (inset in Fig. 2a). This value is larger than that of an ideal diode ($n = 1$), which may be attributed to the higher current leakage caused by the huge amount of defects within the SiNW array/Cu Schottky junction. In fact, the above rectifying characteristics can be understood by the energy band diagram of the Si/Cu Schottky junction shown in Fig. 2b. When Si and Cu was in contact, the energy band of Si near the metal/semiconductor interface will be bent upwards and the electrons will be depleted in the near-surface area of Si, leading to the formation of a built-in electric field near the Si/Cu interface. Owing to the existence of this built-in electric field, the Si/Cu interface will allow the current to move in a one-way fashion, namely it shows typical rectifying behavior.

Theoretically, one may learn from the above diagram that when irradiated by photons with sufficient energy, electron–hole pairs generated in Si will diffuse to the Si/Cu interface and then be separated by the built-in electric field. Consequently, the photo-generated electrons will be preferentially collected by the bottom In/Ga electrode while the photo-generated holes will be injected into the Cu electrode, resulting in a photocurrent. To validate this assumption, we then studied the optoelectronic characteristics of the as-fabricated core–shell SiNW array/Cu Schottky junction illuminated with 980 nm light (0.22 mW cm^{-2}). As shown in Fig. 3a, the device indeed exhibits obvious photocurrent under NIR illumination, with an open-circuit voltage (V_{OC}), a short-circuit current (I_{SC}) and a fill factor (FF) of 0.3 V, 16.2 μA, and 29%, respectively. Although the power conversion efficiency (η) is relatively low ($\sim$2.56%), the present core–shell SiNW array/Cu Schottky junction is able to work as a zero-powered NIR detector without an external power supply. Further analysis of the photoresponse characteristics of the heterojunction under light illumination of different intensities reveals that the photocurrent increases almost linearly with the increase of the light intensity from 0.22 to 6.87 mW cm^{-2} (Fig. 3b and c). Fig. 3d shows the quantitative analysis of the relationship between photocurrent and light intensity which was fitted with a power law $I_p = AP^{\theta}$, where A is a constant for a NIR light, P is the power of NIR illumination and the exponent θ ($0.5 < \theta < 1$) determines the response of photocurrent to the intensity of NIR light, which is fitted to be about 0.67.[18] According to previous study,[19] such a deviation from linear relationship ($\theta = 1$) may be attributed to the defects species in the device which are formed during the etching process.

To evaluate the current NIR photodetector in a more quantitative way, other two key metrics, responsivity (R, defined as the photocurrent generated by per unit of incident power) and detectivity (D^*, normalized to the active detector area and the equivalent noise bandwidth) were calculated by using the following relations:[20]

$$R(\mathrm{A\,W^{-1}}) = \frac{I_p - I_d}{SP_{in}}$$

$$D^* = R\sqrt{\frac{S}{2qI_d}}$$

where I_p is the photocurrent, I_d the dark current, S the effective area of the Si substrate used for the etching of SiNW arrays (0.25 cm^2), P_{in} the incident light power, and q the electron charge (1.6×10^{-19} C). Fig. 3e plots both R and D^* of the core–shell SiNW array/Cu nanofilm Schottky junction at different NIR intensities. It is clear that the responsivity decreases with increasing light intensity (Fig. 3e). This finding is consistent with previous study,[21] and may be attributed to the trap states in the SiNW array or at the junction interface. At weak light intensity, the photogenerated electrons in Si will be captured by the trap states. As a result of reduced recombination, the lifetime of the photogenerated holes can be greatly prolonged, leading to higher R and D^*. When the light intensity increases, however, the available states will be remarkably reduced, causing the saturation of photoresponse.[22] To compare the device performance of the present device with other SiNW based devices, Table 1 summarizes several key metrics including R, D^*, on/off ratio, and response speed. It is apparent that all parameters are comparable to or even higher than that of other photodetectors made of not only the SiNW array–semiconductor heterojunction,[11,17,23]

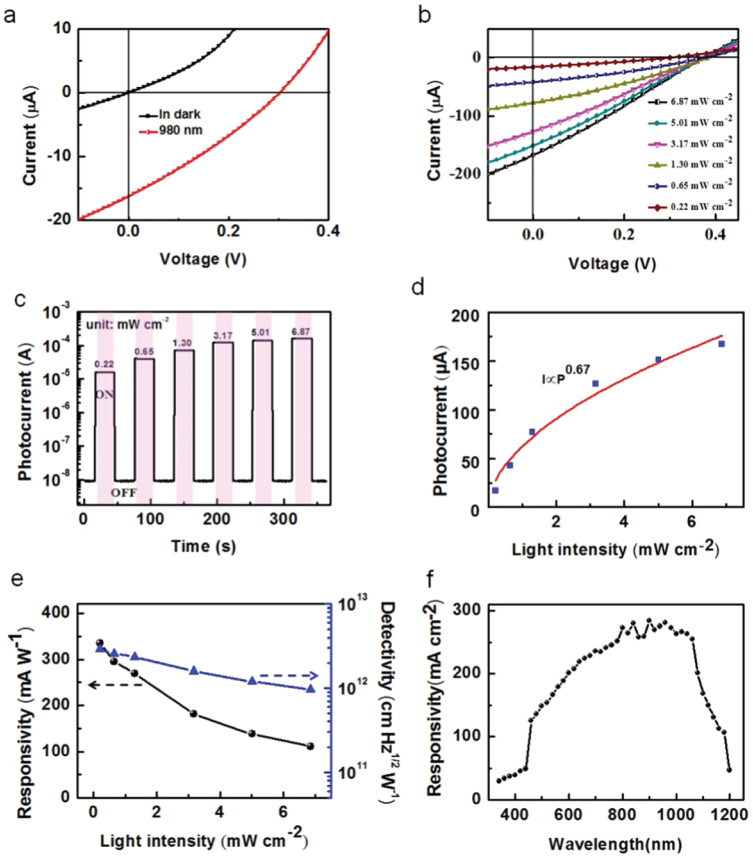

Fig. 3 (a) Electrical characteristics of the core–shell SiNW array/Cu Schottky junction in the dark and illuminated with 980 nm light (0.22 mW cm^{-2}). (b) Photovoltaic characteristics and (c) photoresponse of the device under light illumination with intensity ranging from 0.22 mW cm^{-2} to 6.87 mW cm^{-2}. (d) A fitting curve of the relationship between the photocurrent and the light intensity according to power law. (e) Plots of responsivity and detectivity at zero bias as a function of light intensity. (f) Spectral response of the NIR photodetector.

Table 1 Summary of the reported performances of Si-based NIR PD with similar device structures

Device structure	R (A W^{-1})	τ_r/τ_f (μs/μs)	On/off	D^* (Jones)	Ref.
SiNW array/Cu	0.335	3.6/14.2	1.8×10^4	2.9×10^{12}	This work
CuO/SiNW arrays	0.64×10^{-4}	60/80	$\sim 10^4$	7.6×10^8	11
SiNW array/CQD	0.353	10/40	3×10^3	—	17
MoO_{3-x}/black Si	—	1/51.4	—	6.29×10^{12}	21
MoS_2/planar Si	0.3	3/40	8×10^3	10^{13}	22
Graphene/planar Si	0.029	93/110	$\sim 10^2$	3.9×10^{11}	10

but also two-dimensional material (*e.g.*, graphene and MoS_2)-planar Si interface,[10,24] suggesting the relatively good device performance. Fig. 3f depicts the spectral response of the device, which shows a broadband spectral selectivity over a wide wavelength range from 460 to 1100 nm with peak sensitivity at around 960 nm, consistent with the intrinsic absorption of the SiNW array.[25]

To further explore the feasibility of the present NIR photodetector for practical application in optical communication and switching, the photoresponse properties to pulsed NIR light were also examined by using a laser diode driven by a signal generator to obtain the pulsed light and an oscilloscope to sense the switching behavior of the photocurrent (see the inset of Fig. 4a). Notably, the as-fabricated device can be reversibly switched between high and low conductance for not only a low frequency of 1 kHz, but also a high frequency of 30 kHz, with excellent reproducibility (Fig. 4a and c). Apart from this, the present NIR photodetector also exhibits good stability even when the device is stored under ambient conditions for 3 months (Fig. 4c). This good air-stability is probably related to the protecting effect of ethylene glycol on the CuNP surface: like other chemicals including citrate[26] and polystyrene–poly(4-vinylpyridine) di-block copolymers,[27] ethylene glycol can function as a protective agent by absorbing on the CuNP surface after the reduction of Cu^{2+} to Cu nanoparticles. As a result, the absorbed molecules will prevent getting oxidized by isolating oxygen from CuNPs. Fig. 4d shows the relative balance $(V_{max} - V_{min})/V_{max}$ as a function of frequency. It is revealed that our device has a slow relative balance decay

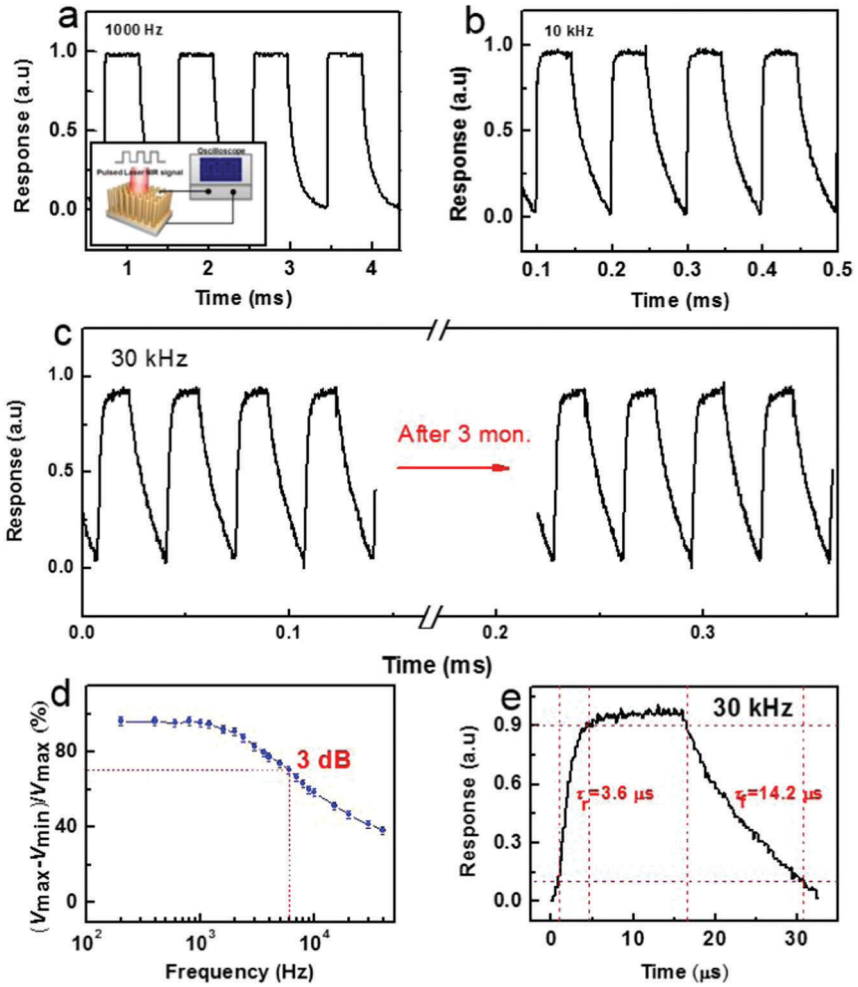

Fig. 4 Photoresponse of the SiNW array/Cu Schottky junction to pulsed NIR light irradiation at different frequencies: (b) 1000 Hz, (c) 10 kHz, the inset in (a) shows the schematic illustration of the measurement configuration for photoresponse speed measurement. (c) Photoresponse of the device under 30 kHz light illumination before and after 3 months of storage. (d) Relative balance $(V_{max} - V_{min})/V_{max}$ *versus* switching frequency. (e) Rising and falling edges for estimating both response and recovery time.

even when the switching frequency reaches 30 kHz. Moreover, the 3 dB-gain bandwidth can be deduced to be about 6 kHz, suggesting that the SiNW array/Cu nanofilm Schottky junction NIR photodetector can work properly over a wide switching frequency range, which is vitally important to monitor the ultrafast optical signal. Meanwhile, the response time (τ_r, defined as the duration needed for the photocurrent to increase from 10 to 90%) and the recovery time (τ_f, defined as the duration needed for the photocurrent to decrease from 90 to 10%) in a switching frequency of 30 kHz was estimated to be 3.6 and 14.2 μs (Fig. 4e). These values are much faster than those of the other reported Si-based photodetectors with similar structures, as summarized in Table 1.

The above optoelectronic characteristics can be ascribed to the obvious advantages in both optical and electrical properties. On one hand, the SiNWs can be regarded as ultimately scaled-down versions of microcylinder resonators that can trap light in circulating orbits by multiple total internal reflections from the periphery. Owing to their small size, the resonant modes in nanowires, usually termed as leaky mode resonance (LMR), become leaky and interact more effectively with the outside world,[28] carrying out a valuable antenna function. When the illumination wavelength matches one of the allowed LMRs, the high refractive index wire was able to capture and trap the light by multiple internal reflections from its boundary. As a consequence, the light absorption could be enhanced, as shown in Fig. 5a. Such a strong light trapping effect is in sharp contrast to the case of planar Si wafer, in which the majority of the incident NIR light will be reflected at the incident interface, and no surface plasmon polariton (SPP) waves are generated (Fig. 5b). In fact, such a difference in light absorption capability is also reflected by their distinction in the reflectance spectrum in which reduced reflectivity is observed on the SiNW array (Fig. 5c). Fig. S4 (ESI†) shows the electrical characteristics under the same illumination conditions (980 nm light, 0.22 mW cm^{-2}). Obviously, although the open-circuit voltage (V_{OC}) is nearly identical to that of a core–shell silicon nanowire–Cu device, the short-circuit current, however, was less than that of the SiNW array/Cu Schottky junction. This relatively poor photovoltaic characteristic is probably due to weak light absorption of the planar Si/Cu

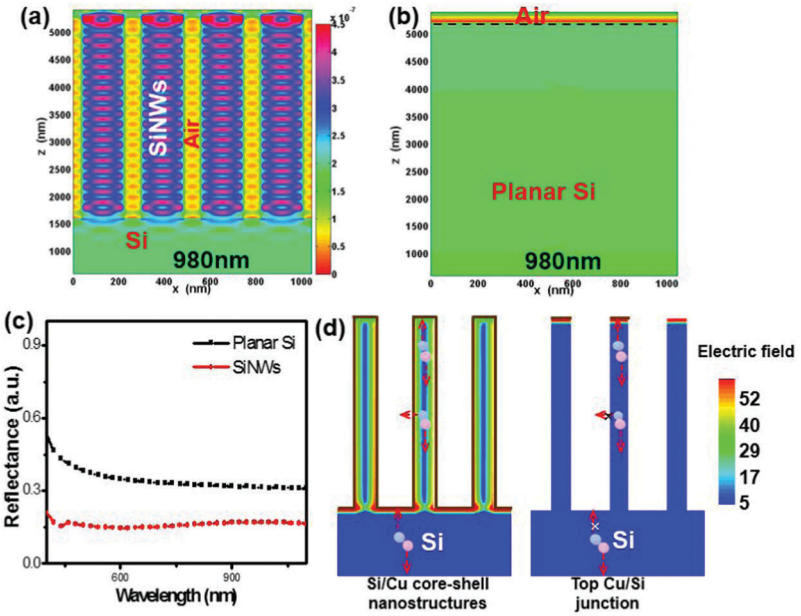

Fig. 5 Simulation of electrical field energy distribution of the Si nanowire array (a) and bulk Si wafer (b) under near infrared light illumination with a wavelength of 980 nm. (c) Reflectance of both SiNW array and planar Si wafer. (d) The simulated electric field distribution at a zero bias of the core–shell SiNW array/Cu Schottky junction (left) and its counterpart with a top Cu electrode (right), respectively.

Schottky junction, as indicated by the theoretical simulation shown in Fig. 5b. In light of this, the contribution of the planar Si/Cu Schottky junction was not considered. On the other hand, the excellent carrier collection ability is due to the huge Schottky junction area. Fig. 5d compares the simulated electrical field distribution of two kinds of devices: one is the present core–shell SiNW array/Cu nanofilm Schottky junction device, and the other is composed of a SiNW array with Cu nanofilm only deposited on the top side. One can see clearly that a large area uniform electric field distributed along the interface exists in the core–shell SiNW array/Cu Schottky junction, which allows for the diffusion of the photo-generated carriers toward the depletion layer within a smaller distance. As for the device with only a top Cu electrode, the electric field has been limited to the top contact area. In this case, only the carriers generated near the top electrode can be successfully separated and collected due to the limited lifetime of the photo-generated carriers. Therefore, a higher efficiency of charge separation and collection can be well expected in the core–shell SiNW array/Cu Schottky junction, implying its potential as a building block for fabricating high performance photodetectors.

Considering the fact that the sensitivity of the NIR detector is highly dependent on the thickness of the Cu nanofilm, we then fabricated several devices that were obtained from different deposition times of the Cu nanofilm. A systematic study of the time dependent thickness of the CuNP nanofilm finds that the growth rate is in the range of 0.5–0.6 nm per min, and the thickness of the nanofilm obtained at 15, 30, and 45 min were estimated to be 7.5–9, 15–18, and 22.5–27 nm, respectively. Fig. 6 shows the *I–V* curves upon illumination, in which photovoltaic characteristics can be observed on all the devices with similar open-circuit voltage (V_{OC}). However, the short-circuit

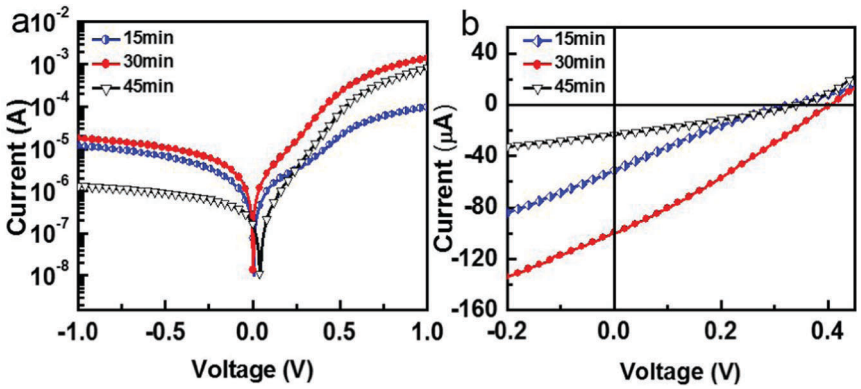

Fig. 6 (a) Typical rectification characteristics in the dark and (b) the corresponding photovoltaic properties of the devices fabricated through different deposition times of the Cu film: 15, 30 and 45 min, respectively.

current (I_{SC}) varies distinctly from 23 to 100 μA and the highest short-circuit current was achieved when the deposition time of the Cu film was 30 min. Such a Cu nanofilm dependent I_{SC} can be understood as follows: when deposited for a relatively shorter time (15 min), Cu nanoparticles with a thickness of 7.5–9 nm may be too small to form a uniform and continuous film around the SiNWs, which greatly hinders the separation and collection of the carriers. Nonetheless, the Cu nanofilm with moderate thickness (*e.g.* the CuNP thin film was formed in 30 min) can form a compact film on the SiNW surface, and thus it has good electrical transport properties, as well as good transparency for light absorption of the SiNWs. Further increase in thickness (the thickness is around 22.5–27 nm when deposited for 45 min) in contrast, begins to reflect much incident light, which undoubtedly reduces the photo-generated carriers.

3. Conclusions

In summary, we have demonstrated the fabrication of a high performance self-powered SiNW array/Cu Schottky junction NIR photodetector by coating a thin layer of Cu film onto the n-type SiNW array. The photodetector exhibits high sensitivity to 980 nm NIR light with responsivity (R) 0.335 A W^{-1}, detectivity (D^*) 2.9 × 10^{12} cm $Hz^{1/2}$ W^{-1} and a fast response speed (response time τ_r 3.6 μs and recovery time τ_f 14.2 μs). Further theoretical simulation reveals that the large area uniform electric field distributed along the NWs may facilitate the separation and collection of the photo-generated carriers and therefore gives rise to the good device performance.

4. Experimental section

Preparation of the SiNW array

The vertically aligned SiNW array was synthesized *via* a silver-assisted HF etching approach from a commercial Si wafer (n-type, (100)-oriented, 4–10 Ω cm).[29] In a typical procedure, a small piece of Si wafer (5 mm × 5 mm in size) cleaned successively in acetone and distilled water was immersed into a solution containing HF (4.8 M) and $AgNO_3$ (0.005 M) for 1 min at room temperature to deposit a layer of Ag nanocatalysts. It was then etched in the mixed solution of 4.8 M HF and 0.3 M H_2O_2 for 20 min. Afterwards, the as-obtained SiNWs were dipped into a diluted HNO_3 and HF solution to etch away Ag and SiO_2 on the SiNW surface, respectively. The SiNW array was then cleaned in deionized water three times and dried under a stream of nitrogen gas.

Device fabrication

In a typical synthesis of the core–shell SiNW array/Cu Schottky junction, 0.06 g $Cu(NO_3)_2{\cdot}3H_2O$ was dissolved into 30 mL deionized water in a 60 mL Teflon-lined stainless steel autoclave to form a homogeneous solution. 4 mL ethylene glycol and 0.5 mL hydrazine hydrate were added into the autoclave sequentially under vigorous stirring. After stirring for about 30 min, the as-etched SiNW array was immersed into the solution. Then the autoclave was sealed and kept at 100 °C for 30 min. After the solution was cooled to room temperature naturally, the SiNW array was taken out and washed with absolute ethanol several times and dried under a stream of nitrogen gas. To prepare the electrode, eutectic In:Ga was pasted onto the reverse of the n-Si substrate for Ohmic contact.[30] What is more, silver paste was placed onto the top side of the SiNW array.

Structural analysis and device characterization

The morphologies and microstructures of the as-etched SiNW array and the core–shell SiNW array/Cu Schottky junction were characterized by X-ray diffraction (XRD, Rigaku D/Max-γB, with Cu Kα radiation), field emission scanning electron microscopy (FESEM, SU8020) and high-resolution transmission electron microscopy (HRTEM, JEOL JEM-2010). Chemical composition analysis was carried out by the energy-dispersive X-ray spectroscopy (EDS, Oxford INCA, attached to FESEM). The optoelectronic characterization of the SiNW array/Cu Schottky junction was carried out at room temperature with a semiconductor characterization system (Keithley 4200-SCS), using a laser diode (980 nm) as the illumination source. A home-built analysis system composed of a laser diode, an oscilloscope (Tektronix, TDS2012B) and a pulse generator was used to investigate the photoresponse properties of the device under light illumination of different pulses. The spectral response was studied using a home-built system composed of a xenon lamp (150 W), a monochromator (Omni-λ300) and a lock-in amplifier (SR830). The device simulation was conducted on a 2D semiconductor simulation package (ISE-TCAD).

Acknowledgements

This work was supported by the Natural Science Foundation of China (NSFC, no. 61575059, 61675062), the Natural Science Foundation of Anhui Province of China (no. 1408085MB31, J2014AKZR0036), and the Fundamental Research Funds for the Central Universities (no. 2012HGCX0003, 2013HGXJ0195, 2013HGCH0012, 2014HGCH0005).

References

1 C. Downs and T. E. Vandervelde, *Sensors*, 2013, **13**, 5054.
2 C. Li, Y. Bando, M. Y. Liao, Y. Koide and D. Golberg, *Appl. Phys. Lett.*, 2010, **97**, 161102.
3 P. C. Wu, Y. Dai, Y. Ye, Y. Yin and L. Dai, *J. Mater. Chem.*, 2011, **21**, 2563.
4 J. F. Wang, M. S. Gudiksen, X. F. Duan, Y. Cui and C. M. Lieber, *Science*, 2001, **293**, 1455.
5 J. S. Jie, W. J. Zhang, K. Q. Peng, G. D. Yuan, C. S. Lee and S. T. Lee, *Adv. Funct. Mater.*, 2008, **18**, 3251.
6 A. Rogalski, *Infrared Phys. Technol.*, 2002, **43**, 187.
7 Y. Cui and C. M. Lieber, *Science*, 2001, **291**, 851.
8 S. M. Sze, *Physics of Semiconductor Devices*, John Wiley & Sons Press, New York, 1981.
9 R. People, J. C. Bean, C. G. Bethea, S. K. Sputz and L. J. Peticolas, *Appl. Phys. Lett.*, 1992, **61**, 1122.

10 P. Lv, X. J. Zhang, X. W. Zhang, W. Deng and J. S. Jie, *IEEE Trans. Electron Devices*, 2013, **34**, 1337.
11 Q. S. Hong, Y. Cao, J. Xu, H. M. Lu, J. H. He and J. L. Sun, *ACS Appl. Mater. Interfaces*, 2014, **6**, 20887.
12 D. S. Tsai, C. A. Lin, W. C. Lien, H. C. Chang, Y. L. Wang and J. H. He, *ACS Nano*, 2011, **5**, 7748.
13 M. Razeghi and A. Rogalski, *J. Appl. Phys.*, 1996, **79**, 7433.
14 T. Zhai, L. Li, X. Wang, X. Fang, Y. Bando and D. Golberg, *Adv. Funct. Mater.*, 2010, **20**, 4233.
15 Y. Cao, J. Y. Zhu, J. Xu, J. H. He, J. L. Sun, Y. X. Wang and Z. R. Zhao, *Small*, 2014, **10**, 2345.
16 L. B. Luo, L. H. Zeng, C. Xie, Y. Q. Yu, F. X. Liang, C. Y. Wu, L. Wang and J. G. Hu, *Sci. Rep.*, 2014, **4**, 3914.
17 C. Xie, B. Nie, L. H. Zeng, F. X. Liang, M. Z. Wang, L. B. Luo, M. Feng, Y. Q. Yu, C. Y. Wu, Y. C. Wu and S. H. Yu, *ACS Nano*, 2014, **8**, 4015.
18 N. V. Joshi, *Photoconductivity: art science and technology*, Marcel Dekker Press, New York, 1990.
19 Y. L. Cao, Z. T. Liu, L. M. Chen, Y. B. Tang, L. B. Luo, J. S. Jie, W. J. Zhang, S. T. Lee and C. S. Lee, *Opt. Express*, 2011, **19**, 6105.
20 J. M. Liu, *Photonic Devices*, Cambridge University Press, New York, 2005.
21 B. D. Boruah, A. Mukherjee and A. Misra, *Nanotechnology*, 2016, **27**, 095205.
22 H. Xu, J. H. Wu, Q. L. Feng, N. N. Mao, C. M. Wang and J. Zhang, *Small*, 2014, **10**, 2300.
23 C. X. Zhao, Z. M. Liang, M. Z. Su, P. Y. Liu, W. J. Mai and W. G. Xie, *ACS Appl. Mater. Interfaces*, 2015, **7**, 25981.
24 L. Wang, J. Jie, Z. Shao, Q. Zhang, X. Zhang, Y. Wang, Z. Sun and S.-T. Lee, *Adv. Funct. Mater.*, 2015, **25**, 2910.
25 F. X. Liang, D. Y. Zhang, Y. F. Zou, H. Hu, T. F. Zhang, Y. C. Wu and L. B. Luo, *RSC Adv.*, 2015, **5**, 19020.
26 C. Kind, A. Weber and C. Feldmann, *J. Mater. Chem.*, 2012, **22**, 987.
27 I. I. Perepichka, M. A. Mezour, D. F. Perepichka and R. B. Lennox, *Chem. Commun.*, 2014, **50**, 11919.
28 L. Y. Cao, P. Y. Fan, A. P. Vasudev, J. S. White, Z. F. Yu, W. S. Cai, J. A. Schuller, S. H. Fan and M. L. Brongersma, *Nano Lett.*, 2010, **10**, 439.
29 K. Q. Peng, H. Fang, J. J. Hu, Y. Wu, J. Zhu, Y. J. Yan and S. T. Lee, *Chem. – Eur. J.*, 2006, **12**, 7942.
30 X. Shen, B. Sun, D. Liu and S. T. Lee, *J. Am. Chem. Soc.*, 2011, **133**, 19408.